Bulletin of the Mineral Research and Exploration

http://bulletin.mta.gov.tr

Magnetic anisotropy of a sub-ophiolitic metamorphic sole (Mersin ophiolite, Türkiye)

Buğra ÇAVDAR[a,b*], Antony MORRIS[b], Mark ANDERSON[b], Luca MENEGON[c] and Osman PARLAK[d]

[a]*General Directorate of Mineral Research and Exploration, Mineral Research and Exploration Department, 06530, Ankara, Türkiye*
[b]*University of Plymouth, School of Geography, Earth and Environmental Sciences, Drake Circus, PL4 8AA, Plymouth, United Kingdom*
[c]*University of Oslo, Department of Geosciences, The Njord Centre, 1048, Blindern, Norway*
[d]*Çukurova University, Faculty of Engineering, Department of Geological Engineering, 01380, Adana, Türkiye*

Research Article

Keywords:
Magnetic Anisotropy, Rock Magnetism, Amphibolites, Ophiolite, Metamorphic Sole.

ABSTRACT

The Mersin ophiolite of southern Turkey is a well-exposed, Late Cretaceous, Neo-Tethyan supra-subduction zone ophiolite. It is underlain by metamorphic sole rocks inferred to have formed at the top of a down-going plate during subduction. These have a well-developed foliation and lineation observable in the field (defined by the preferred orientations of hornblende and plagioclase crystals). Here we present the first magnetic fabric data reported from the Mersin ophiolite with such settings. Anisotropy of low field magnetic susceptibility ellipsoids in sampled amphibolites have clustered, NW-plunging minimum principal axes representing poles to a SE-dipping magnetic foliation that aligns with the macroscopic metamorphic foliation plane seen in the field. Maximum AMS principal axes define a SE-plunging magnetic lineation that is parallel to the macroscopic metamorphic lineation. Oblate magnetic fabrics at specimen-level and an overall triaxial fabric at locality-level in these rocks are consistent with the development of the dominant metamorphic fabric by a combination of pure shear flattening and simple shearing during the formation and exhumation of the Mersin sole rocks. These observations are compatible with a recent tectonic model for the evolution of the ophiolite based on paleomagnetic data that invokes flattening and exhumation of the down-going slab in an incipient subduction zone during supra-subduction zone spreading.

Received Date: 12.07.2021
Accepted Date: 29.11.2021

1. Introduction

Magnetic fabric analysis has proved to be a valuable tool in understanding the structural evolution of rocks in a wide variety of geological settings (Tarling and Hrouda, 1993; Martín Hernández et al., 2004; Parés, 2015). Anisotropy of magnetic susceptibility (AMS) reflects the shape- or crystallographic-preferred orientations of minerals and grains in rock (Tarling and Hrouda, 1993; Borradaile and Jackson, 2004), or the distribution anisotropy of ferromagnetic grains (Stephenson, 1994), providing quantitative constraints on petrofabric development even in weakly deformed rocks. Described by a second-order tensor, AMS is represented by a susceptibility ellipsoid specified by the magnitude and orientation of its principal axes (k_{max}, k_{int} and k_{min}, corresponding to its maximum, intermediate, and minimum susceptibility axes, respectively). AMS in a rock results from contributions from all its constituent minerals but is usually dominated by the signal from ferromagnetic phases when present because of their high susceptibilities.

Much attention has been given to using AMS to understand the development of fabrics in sedimentary and igneous rocks, and such studies have therefore

Citation Info: Çavdar, B., Morris, A., Anderson, M., Menegon, L., Parlak, O. 2023. Magnetic anisotropy of a sub-ophiolitic metamorphic sole (Mersin ophiolite, Türkiye). Bulletin of the Mineral Research and Exploration 170, 1-14. https://doi.org/10.19111/bulletinofmre.1081170

**Corresponding author: Buğra ÇAVDAR, bugra.cavdar@mta.gov.tr*

dominated the literature on magnetic fabrics. For example, k_{max} axes are a reliable proxy for extension directions in weakly deformed sedimentary rocks that lack macroscopic strain markers (Borradaile and Hamilton, 2004; Mattei et al., 2004) and for magmatic flow directions in volcanic (Morris, 2000; Cañón Tapia, 2004) and plutonic rocks (Bouchez, 1997; Staudigel et al., 1999; Morris et al., 2019). In contrast, AMS has been relatively underutilised as a tool in the analysis of metamorphic rocks, although several studies have successfully used magnetic fabric analysis to provide new insights into the kinematics of fabric development in higher-grade rocks such as mylonites (Bascou et al., 2002) and migmatites (Ferré et al., 2003, 2004; Kruckenberg et al., 2010).

Here we present the first AMS data reported from the metamorphic sole of an ophiolite as part of a wider magnetic project on the tectonic history of the Mersin ophiolite of southern Türkiye (Omer, 2014; Morris et al., 2017). These amphibolite-grade rocks have well-defined macroscopic fabrics (Parlak et al., 1996) that developed during their evolution as they have subducted beneath a Neotethyan supra-subduction zone seafloor spreading system and later exhumed and accreted to the base of the overlying Mersin ophiolite (Parlak et al., 1995). We show that AMS in these rocks provides an accurate proxy for the orientation of the macroscopic foliation and lineation observed in the field and indicates an important flattening component. These new magnetic fabric constraints on fabric development are consistent with a recent tectonic model for the evolution of the Mersin ophiolite (Morris et al., 2017), based on net tectonic rotation analysis of paleomagnetic data that predicts shearing and flattening of the sole rocks in an incipient subduction zone system.

2. The Mersin Ophiolite and its Metamorphic Sole

The Mersin ophiolite outcrops over a 1500 km^2 area in southern Türkiye (Figure 1a) and consists of a Late Cretaceous ophiolite underlain by metamorphic sole rocks that overlie the Mersin Mélange (Figure 1b; Parlak and Delaloye, 1996, 1999; Parlak and Robertson, 2004; Parlak et al., 2013). The ophiolitic suite consists mainly of the mantle and lower crustal sequences, including tectonised harzburgites and ultramafic and mafic cumulate gabbros (Parlak et al., 1996). Thin, fine-grained basaltic dykes occasionally

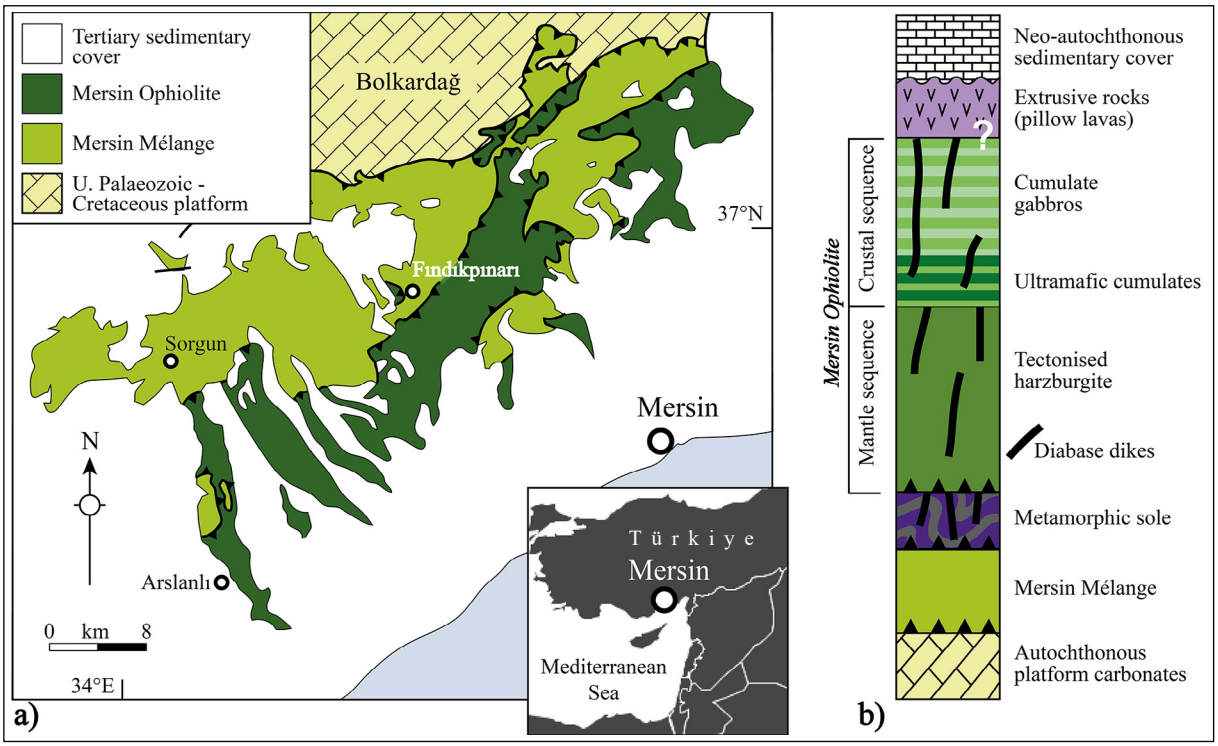

Figure 1- Summary of the geology of the Mersin ophiolite of southern Türkiye and location of the study near the village of Fındıkpınarı; a) the simplified geological map is after Tekin et al. (2016), b) the tectonostratigraphic column is after Parlak et al. (1996).

intrude the gabbros at a high angle to the cumulate layering. Basalts and associated deep marine sediments are structurally isolated from the main ophiolitic body (Parlak et al., 1996).

Key sections through the metamorphic sole and mantle sequence are exposed in the Fındıkpınarı valley area (Figure 1a). Here, the sole has sharp tectonic contact with the overlying mantle sequence (Figure 2a). It consists predominantly of amphibolites, amphibolitic schists, epidote-amphibolite schists, quartz-mica schists, calcschists, and marble. Over a thickness of about 50-70 m from top to base, it displays a typical inverted metamorphic zonation from upper amphibolite (top) to greenschist facies (base) (Parlak et al., 1996). The upper part of the Fındıkpınarı section is dominated by amphibolites, with phyllitic rocks and foliated metabasalts (accompanied by subordinate lenses of amphibolite) becoming more frequent towards the base. Intense deformation fabrics within the metamorphic sole are inferred to have formed along with the upper interface of a subducting slab. A pervasive SE-dipping metamorphic foliation (mean dip direction/dip = 146°/45°; Figure 2b) is associated with a mostly NW-SE-trending lineation (mean azimuth/plunge= 133°/46°) within the foliation plane, defined principally by alignment of elongate amphibole crystals.

The metamorphic sole and tectonised harzburgite are both occasionally cut by undeformed doleritic dykes that compositionally resemble evolved island-arc tholeiites derived from a mantle wedge that underwent previous melt extraction and subsequent metasomatism (Dilek et al., 1999). Dykes intruding the metamorphic sole clearly post-date shearing and metamorphism. ^{40}Ar–^{39}Ar age constraints (Dilek et al., 1999; Parlak and Delaloye, 1996, 1999) indicate that cooling of the metamorphic sole through amphibolite facies conditions (mean age= 92.7 Ma), intrusion of dykes into the mantle sequence (91.0 Ma), and intrusion of dykes through the sole (mean age= 89.6 Ma) were broadly synchronous events. Paleomagnetic analysis of the metamorphic sole-hosted dykes, those in the mantle sequence, and the overlying lower crustal cumulate gabbros reveals that each unit underwent large clockwise net tectonic rotations around similar NE-trending, shallowly plunging inclined axes. However, dykes in the sole experienced only about 45° rotation compared to about 120-125° rotation of the overlying mantle-hosted dykes and cumulate gabbros (Morris et al., 2017). These data support a model involving rotation of the Mersin oceanic crust and related mantle rocks in the footwall of a Neotethyan oceanic detachment fault system (Morris et al., 2017), with a later phase of footwall rotation occurring around the same ridge-parallel axis after accretion of the metamorphic sole rocks to the base of the footwall.

3. Sampling and Methods

We sampled amphibolites and some mica schists of the metamorphic sole of the Mersin ophiolite at 11

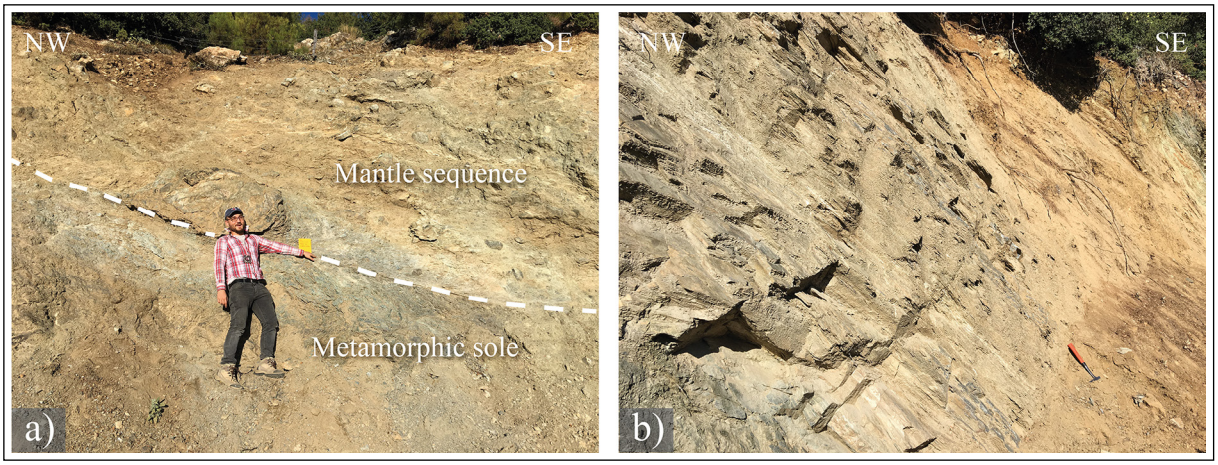

Figure 2- Field photographs of the metamorphic sole of the Mersin ophiolite exposed along the road-cut section near Fındıkpınarı; a) the tectonic contact between the metamorphic sole and the overlying mantle sequence of the ophiolite, b) amphibolites of the metamorphic sole showing the pronounced SE-dipping metamorphic foliation (hammer for scale).

sites distributed along a 650 m long road cut section near the village of Fındıkpınarı (Figure 1a, Table 1). At each site, oriented hand samples were collected and then drilled in the laboratory to obtain an average of eight standards (11 cm^3) cylindrical specimens per site for AMS analyses. Sampling was restricted to exposures that showed well-developed planar foliations. The orientations of foliations and lineations were measured to an accuracy of ± 5°.

Table 1- Site locations with the metamorphic sole rocks of the Mersin ophiolite.

Site	Lithology	UTM location
BC02	Amphibolite	36S 619297E, 4083374N
BC03	Amphibolite	36S 619238E, 4083392N
BC04	Amphibolite	36S 619251E, 4083390N
BC07	Amphibolite	36S 619330E, 4083355N
BC08	Amphibolite	36S 619097E, 4083484N
BC09	Amphibolite	36S 618959E, 4083576N
BC10	Amphibolite	36S 618915E, 4083598N
BC11	Micaschist/ Amphibolite	36S 618910E, 4083608N
BC12	Amphibolite	36S 618870E, 4083667N
BC13	Amphibolite	36S 618848E, 4083764N
BC14	Micaschist	36S 618836E, 4083777N

The anisotropy of low-field magnetic susceptibility of 96 specimens was measured using an AGICO-KLY-3S Kappabridge instrument. AMS tensors and associated eigenvectors and eigenvalues were calculated at specimen-level using AGICO SUSAR software. The shape of the AMS ellipsoid is defined by the relative magnitude of the principal susceptibility axes and can be: 1) isotropic ($k_{min} = k_{int} = k_{max}$) with no preferred alignment; 2) oblate ($k_{min} << k_{int} \approx k_{max}$) defining a planar magnetic fabric (foliation); 3) prolate ($k_{min} \approx k_{int} << k_{max}$) defining a linear magnetic fabric (lineation); or 4) triaxial ($k_{min} < k_{int} < k_{max}$). The magnitude of anisotropy is described using the corrected anisotropy degree, P_J (Jelínek, 1981), where $P_J = 1.0$ indicates an isotropic fabric and, e.g., $P_J = 1.05$ indicates 5% anisotropy. The shape parameter (T) describes the shape of the ellipsoid ($-1.0<T<1.0$), with positive/negative values of T indicating oblate/prolate fabrics, respectively (Jelínek, 1981). Statistical analysis of the data at the locality level was achieved using the bootstrap method of Constable and Tauxe (1990).

Rock magnetic experiments were performed on representative powdered samples to investigate the nature of the ferromagnetic minerals contributing to the AMS. Curie temperatures were determined from the high-temperature (20-700°C) variation of magnetic susceptibility, measured using an AGICO KLY-3S Kappabridge coupled with an AGICO CS-3 high-temperature furnace apparatus. These data were analysed using AGICO Cureval8 software. Isothermal remanent magnetisation (IRM) acquisition experiments were conducted on representative samples using a Molspin pulse magnetiser to apply peak fields up to 800 mT with resulting IRMs measured using an AGICO JR6A fluxgate spinner magnetometer. Scanning electron microscopy and optical microscopy of oriented thin sections were used to further constrain the source of the AMS.

4. Findings

4.1. Rock Magnetic Properties

Bulk low field susceptibility values of the metamorphic sole rocks range between 0.38 x 10^{-3} SI and 7.85 x 10^{-3} SI (mean= 1.15 x 10^{-3} SI; Figure 3), suggesting that paramagnetic minerals dominate the AMS signal (Tarling and Hrouda, 1993) with a minor contribution from ferromagnetic minerals (Figure 3). This is confirmed by the temperature variations of low field magnetic susceptibility (Figure 4) that are dominated by a hyperbolic paramagnetic decay curve following the Curie-Weiss Law (Tarling and Hrouda, 1993), followed by a more rapid decrease in susceptibility at around 560-580°C, suggesting the presence of magnetite. Paramagnetic/ferromagnetic separation based on hyperbola fitting performed using AGICO Cureval8 software (green dashed lines in Figure 4) suggests that 90% of the susceptibility signal is due to paramagnetic minerals. Susceptibilities are systematically higher during the cooling cycle in these experiments and typically display an additional inflection at ~500°C that is not present during the heating cycle.

This suggests the production of new magnetite from a paramagnetic precursor mineral resulting from alteration during heating. IRM acquisition

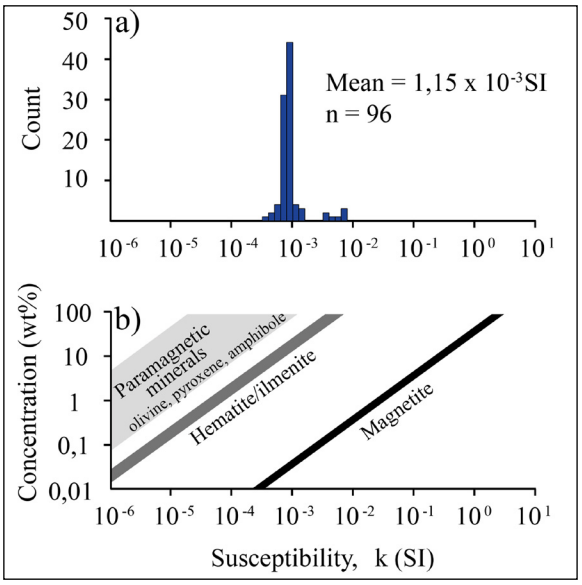

Figure 3- a) Histogram of low-field magnetic susceptibilities for amphibolites of the metamorphic sole of the Mersin ophiolite, b) relationship between bulk susceptibility and mineral concentrations (wt percent, Tarling and Hrouda, 1993). Note that low susceptibilities indicate less than 0.1 wt percent magnetite in most of these rocks and a major contribution from paramagnetic silicate minerals.

curves (Figure 4) reach saturation in most samples by applied fields of 300 mT, suggesting the presence of fine-grained, acicular magnetite. However, some samples (e.g. BC0303A and BC0401B in Figure 4) do not saturate in the maximum applied field of 800 mT suggesting the presence of high coercivity hematite. Maximum IRM intensities are typically less than 400 mAm^{-1}, consistent with the presence of only minor quantities of ferromagnetic minerals in these rocks. These values are also lower than those typically reported from mafic igneous rocks, e.g. within the overlying ophiolite, where IRM_{800mT} values of ~50 Am^{-1} are observed (Omer, 2014; Morris et al., 2017), suggesting a reduction in the concentration of ferromagnetic phases during metamorphism of the original basaltic protoliths of the amphibolites (Parlak et al., 1996). This probably reflects the destruction of primary igneous magnetite during alteration, mobilising iron that became incorporated into newly formed amphibole crystals, as reported recently from the Thetford Mines ophiolite, Canada (Di Chiara et al., 2020). It is also noted that magnetite minerals can also be produced by the breakdown of pyrite at 370°C.

4.2. Magnetic Anisotropy Results

Specimen-level AMS data and derived parameters are provided in Table 2. Corrected anisotropy degrees (P_J) range from 1.01 to 1.13, with a mean value of 1.04 (indicating 4% anisotropy). There is a statistically significant positive correlation between P_J and $\log_{10}$ susceptibility (Figure 5a), excluding data from site

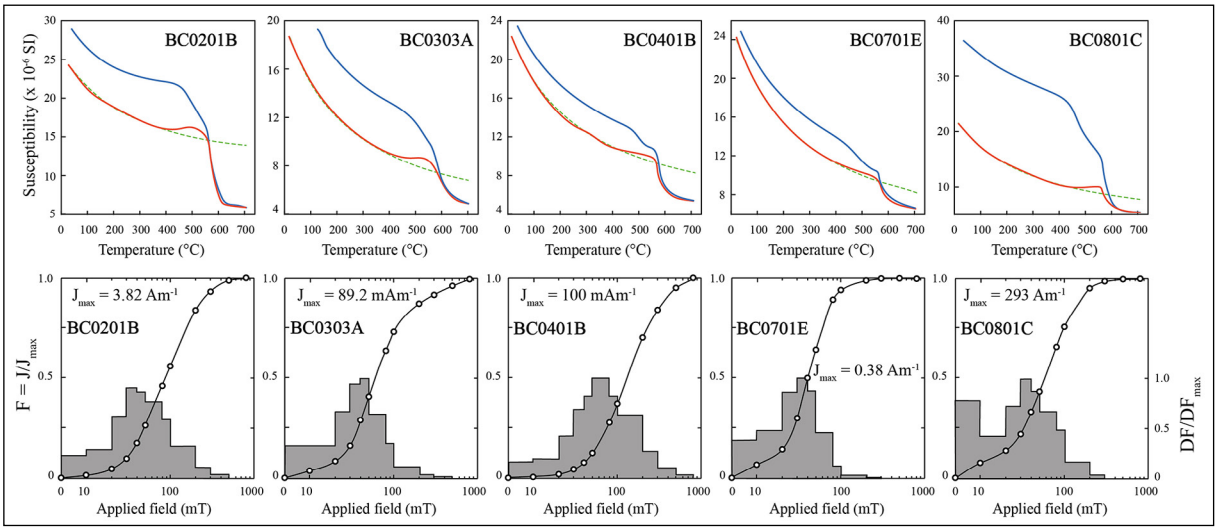

Figure 4- Representative plots showing the variation of low-field magnetic susceptibility with temperature (upper row) and isothermal remanent magnetisation acquisition curves (lower row) for metamorphic sole rocks of the Mersin ophiolite. Note that histograms in the lower row indicate the rate of change in acquired magnetization. The bar charts of BC0201B, BC0701E and BC0801C samples suggest that the saturation is reached around 300 mT of the applied field. However, BC0303A and BC0401B samples do not still saturate in the field of 800 mT, indicating the presence of high coercivity hematite.

Table 2- Anisotropy of magnetic susceptibility (AMS) results from the metamorphic sole rocks of the Mersin ophiolite.

Site	Specimen	Lithology	Mean susceptibility (SI)	Normalised k_{max}	Normalised k_{int}	Normalised k_{min}	Corrected anisotropy degree, Pj	Shape parameter, T	AMS principal axes (geographic coordinates)		
									k_{max}	k_{int}	k_{min}
BC02	BC0201A1	Amphibolite	9.40E-04	1.0314	0.935	1.121	1.0336	0.956	259/22	099/67	352/07
BC02	BC0201A2	Amphibolite	7.81E-04	1.0298	0.9366	1.118	1.0336	0.926	081/18	235/70	349/08
BC02	BC0201B1	Amphibolite	1.03E-03	1.0279	0.9403	1.111	1.0318	0.919	265/15	078/75	174/02
BC02	BC0201B2	Amphibolite	6.87E-04	1.0278	0.9396	1.112	1.0326	0.902	264/12	086/78	354/01
BC02	BC0202A	Amphibolite	1.55E-03	1.0186	0.8981	1.211	1.0832	0.344	233/15	108/65	329/20
BC02	BC0202B	Amphibolite	1.38E-03	1.021	0.9106	1.179	1.0684	0.432	099/53	242/31	343/18
BC02	BC0203A	Amphibolite	9.11E-04	1.008	0.9665	1.063	1.0255	0.417	162/49	071/01	341/41
BC02	BC0203B1	Amphibolite	9.00E-04	1.0086	0.9647	1.066	1.0268	0.427	208/24	070/59	307/18
BC02	BC0203B2	Amphibolite	9.26E-04	1.008	0.9653	1.065	1.0267	0.405	209/22	071/61	306/17
BC02	BC0203C1	Amphibolite	7.64E-04	1.0097	0.9644	1.066	1.0259	0.486	167/47	071/05	337/42
BC02	BC0203C2	Amphibolite	9.06E-04	1.0066	0.9686	1.059	1.0248	0.366	169/49	074/04	340/41
BC02	BC0204A	Amphibolite	8.48E-04	1.0332	0.9258	1.14	1.0409	0.873	043/05	137/42	308/47
BC02	BC0204B	Amphibolite	8.85E-04	1.0414	0.9117	1.17	1.0468	0.925	213/05	118/44	308/45
BC02	BC0204C	Amphibolite	8.65E-04	1.0412	0.9145	1.164	1.0443	0.955	048/12	150/43	306/44
BC03	BC0301A	Amphibolite	7.48E-04	1.0083	0.9763	1.043	1.0154	0.64	116/49	225/16	327/37
BC03	BC0301C	Amphibolite	7.32E-04	1.0074	0.9767	1.042	1.0159	0.573	116/46	225/17	330/39
BC03	BC0301D	Amphibolite	6.93E-04	1.008	0.9765	1.042	1.0155	0.621	125/46	230/13	331/40
BC03	BC0301E	Amphibolite	7.63E-04	1.0055	0.9823	1.032	1.0121	0.562	119/47	225/14	327/40
BC03	BC0301F	Amphibolite	7.64E-04	1.004	0.9815	1.034	1.0145	0.374	117/44	223/16	327/42
BC03	BC0301G	Amphibolite	3.82E-04	1.0077	0.9743	1.047	1.018	0.536	121/43	225/15	329/44
BC03	BC0301H	Amphibolite	7.64E-04	1.0029	0.9848	1.028	1.0123	0.323	117/45	228/19	334/38
BC03	BC0301I	Amphibolite	6.78E-04	1.0077	0.9778	1.04	1.0146	0.631	121/47	223/11	323/41
BC03	BC0301J	Amphibolite	7.49E-04	1.0026	0.9843	1.03	1.0132	0.273	094/36	206/27	323/42
BC03	BC0301K	Amphibolite	4.29E-04	1.011	0.9697	1.055	1.0192	0.676	130/53	231/08	327/36
BC03	BC0301L	Amphibolite	7.17E-04	1.0078	0.9762	1.043	1.016	0.596	141/53	234/03	326/37
BC03	BC0301M	Amphibolite	7.31E-04	1.0058	0.9792	1.038	1.0151	0.488	130/53	235/11	333/35
BC03	BC0302A	Amphibolite	7.45E-04	1.0066	0.9807	1.035	1.0127	0.627	122/56	226/10	322/33
BC03	BC0302B	Amphibolite	7.62E-04	1.0086	0.9768	1.042	1.0145	0.691	124/54	227/09	324/35
BC03	BC0302C	Amphibolite	8.29E-04	1.0123	0.9691	1.056	1.0186	0.748	121/54	223/09	320/35
BC03	BC0302D	Amphibolite	7.67E-04	1.0088	0.9761	1.043	1.0151	0.684	121/54	226/11	323/34
BC04	BC0401A1	Amphibolite	7.98E-04	1.0089	0.9718	1.052	1.0193	0.571	139/45	236/07	333/44
BC04	BC0401A2	Amphibolite	8.23E-04	1.0095	0.9692	1.057	1.0213	0.557	145/45	242/07	339/44
BC04	BC0401B1	Amphibolite	8.35E-04	1.0099	0.968	1.059	1.022	0.561	136/46	237/10	336/42
BC04	BC0401B2	Amphibolite	7.96E-04	1.0071	0.9764	1.043	1.0165	0.542	144/50	236/02	327/40
BC04	BC0401C1	Amphibolite	7.92E-04	1.0124	0.9652	1.064	1.0224	0.658	144/43	236/02	328/47
BC04	BC0401C2	Amphibolite	7.98E-04	1.0096	0.9678	1.059	1.0226	0.536	157/45	063/05	328/44
BC04	BC0401D1	Amphibolite	7.78E-04	1.009	0.9693	1.057	1.0217	0.527	149/48	240/01	331/42

Table 2- continued

BC04	BC0401D2	Amphibolite	7.47E-04	1.011	0.9696	1.055	1.0194	0.672	163/50	062/09	324/39
BC04	BC0401E1	Amphibolite	8.17E-04	1.0094	0.9715	1.052	1.0191	0.598	153/50	061/01	330/40
BC04	BC0401E2	Amphibolite	8.42E-04	1.012	0.9642	1.066	1.0238	0.611	145/48	237/02	329/42
BC04	BC0401E3	Amphibolite	6.39E-04	1.0128	0.96	1.074	1.0272	0.583	138/47	237/08	334/42
BC04	BC0401F1	Amphibolite	8.11E-04	1.0131	0.9623	1.069	1.0246	0.641	138/46	235/06	331/43
BC04	BC0401F2	Amphibolite	8.48E-04	1.0064	0.9755	1.045	1.018	0.463	150/47	243/03	336/43
BC04	BC0401F3	Amphibolite	6.08E-04	1.0136	0.9589	1.076	1.0275	0.606	133/45	233/10	333/43
BC04	BC0401G1	Amphibolite	8.66E-04	1.0095	0.9685	1.058	1.022	0.541	151/45	243/01	334/45
BC04	BC0401G2	Amphibolite	7.98E-04	1.0119	0.9672	1.06	1.0209	0.671	155/47	062/03	329/43
BC04	BC0401G3	Amphibolite	5.36E-04	1.0108	0.9645	1.066	1.0247	0.548	139/45	235/06	331/44
BC07	BC0701B1	Amphibolite	9.31E-04	1.0297	0.9323	1.127	1.038	0.85	212/48	108/12	008/40
BC07	BC0701B2	Amphibolite	7.55E-04	1.0211	0.9518	1.088	1.0271	0.846	211/48	111/10	012/40
BC07	BC0701B3	Amphibolite	8.22E-04	1.0341	0.9244	1.143	1.0414	0.882	185/54	278/03	010/36
BC07	BC0701C1	Amphibolite	8.62E-04	1.0265	0.9417	1.108	1.0317	0.889	201/52	101/07	006/37
BC07	BC0701C2	Amphibolite	9.40E-04	1.0313	0.9256	1.141	1.0431	0.809	153/61	276/17	013/23
BC07	BC0701C3	Amphibolite	8.19E-04	1.0288	0.9316	1.129	1.0396	0.811	164/43	264/11	005/45
BC07	BC0701D1	Amphibolite	8.81E-04	1.0339	0.9236	1.145	1.0425	0.864	154/62	268/12	003/25
BC07	BC0701D2	Amphibolite	8.67E-04	1.0275	0.9375	1.117	1.035	0.854	139/32	252/31	015/42
BC07	BC0701D3	Amphibolite	8.14E-04	1.0285	0.9366	1.118	1.0348	0.877	164/49	270/14	011/38
BC07	BC0701E1	Amphibolite	7.96E-04	1.0364	0.9161	1.161	1.0476	0.84	160/51	270/15	011/35
BC07	BC0701E2	Amphibolite	8.75E-04	1.0294	0.9377	1.116	1.0329	0.929	184/52	277/03	009/38
BC07	BC0701E3	Amphibolite	8.81E-04	1.0358	0.9203	1.152	1.0439	0.877	175/62	270/03	002/27
BC08	BC0801A1	Amphibolite	7.68E-04	1.016	0.9569	1.079	1.027	0.696	096/47	191/05	286/43
BC08	BC0801A2	Amphibolite	8.27E-04	1.0182	0.9502	1.092	1.0315	0.683	112/44	017/05	282/46
BC08	BC0801B	Amphibolite	7.47E-04	1.016	0.9582	1.077	1.0258	0.716	086/42	187/12	289/46
BC08	BC0801C1	Amphibolite	7.57E-04	1.0173	0.9568	1.079	1.026	0.756	098/44	193/05	289/46
BC08	BC0801C2	Amphibolite	5.63E-04	1.0151	0.959	1.075	1.0258	0.688	099/45	192/03	286/45
BC09	BC0901A	Amphibolite	6.40E-04	1.009	0.968	1.059	1.023	0.5	115/45	206/02	298/45
BC09	BC0901B	Amphibolite	5.35E-04	1.0069	0.9723	1.051	1.0207	0.44	132/46	038/04	304/44
BC09	BC0901C	Amphibolite	6.64E-04	1.0082	0.9693	1.057	1.0226	0.471	112/40	213/13	317/47
BC09	BC0902A1	Amphibolite	4.75E-03	1.013	0.8751	1.273	1.1118	0.222	100/48	203/12	303/40
BC09	BC0902A2	Amphibolite	3.14E-03	1.0123	0.8636	1.304	1.1241	0.205	108/46	211/12	312/41
BC09	BC0902B	Amphibolite	1.28E-03	1.0067	0.9731	1.05	1.0202	0.438	083/34	194/27	313/43
BC09	BC0902C	Amphibolite	3.33E-03	1.0438	0.8269	1.383	1.1294	0.495	115/42	222/18	329/43
BC10	BC1001A	Amphibolite	1.11E-03	1.0346	0.8978	1.203	1.0676	0.638	176/28	074/21	313/54
BC10	BC1001B	Amphibolite	9.35E-04	1.0268	0.9163	1.163	1.057	0.595	100/39	206/19	316/45
BC10	BC1002A	Amphibolite	7.59E-04	1.0301	0.9352	1.121	1.0346	0.914	045/23	299/33	162/48
BC10	BC1002B	Amphibolite	7.69E-04	1.0295	0.935	1.122	1.0356	0.885	027/36	282/19	170/48
BC10	BC1002C	Amphibolite	8.44E-04	1.0251	0.9466	1.098	1.0283	0.924	003/41	264/10	164/48

Table 2- continued

BC10	BC1002D	Amphibolite	7.21E-04	1.0275	0.9388	1.114	1.0337	0.874	027/36	282/20	168/47
BC10	BC1002E	Amphibolite	7.81E-04	1.029	0.9374	1.117	1.0337	0.907	027/35	283/19	170/49
BC10	BC1002F	Amphibolite	9.40E-04	1.0221	0.9501	1.092	1.0277	0.861	005/43	265/11	163/45
BC10	BC1002G	Amphibolite	1.13E-03	1.0236	0.9486	1.095	1.0278	0.896	007/43	266/11	164/45
BC11	BC1101A1	Micaschist/ Amphibolite	6.96E-04	1.0274	0.9383	1.115	1.0343	0.864	040/30	289/32	163/43
BC11	BC1101A2	Micaschist/ Amphibolite	9.78E-04	1.0441	0.8866	1.226	1.0693	0.746	025/39	274/24	161/42
BC11	BC1101B	Micaschist/ Amphibolite	1.06E-03	1.0506	0.8795	1.242	1.0699	0.814	026/41	275/23	164/41
BC11	BC1101E	Micaschist/ Amphibolite	8.26E-04	1.0483	0.8761	1.25	1.0756	0.749	026/37	274/26	158/42
BC12	BC1201A	Amphibolite	6.15E-03	1.0141	0.905	1.197	1.0809	0.282	110/51	212/09	310/37
BC12	BC1201B	Amphibolite	6.31E-03	1.0154	0.9109	1.182	1.0736	0.322	109/42	212/13	315/45
BC12	BC1201C	Amphibolite	6.69E-03	1.0166	0.9045	1.196	1.0789	0.326	115/47	216/10	315/41
BC12	BC1201D	Amphibolite	7.85E-03	1.0204	0.8974	1.211	1.0822	0.371	109/50	212/11	311/37
BC13	BC1301A	Amphibolite	7.88E-04	1.0249	0.9415	1.109	1.0336	0.819	119/18	217/23	355/61
BC13	BC1301B	Amphibolite	8.48E-04	1.0247	0.942	1.108	1.0333	0.818	113/15	210/27	357/59
BC13	BC1301C	Amphibolite	8.55E-04	1.0283	0.9338	1.124	1.0379	0.823	111/15	210/31	359/55
BC14	BC1401A	Micaschist	7.63E-04	1.0271	0.9329	1.126	1.04	0.772	127/03	219/31	032/59
BC14	BC1401B	Micaschist	4.15E-04	1.0186	0.9485	1.096	1.0328	0.675	293/12	196/32	041/55
BC14	BC1402A	Micaschist	8.80E-04	1.0278	0.9359	1.12	1.0363	0.839	253/12	158/22	009/64
BC14	BC1402B	Micaschist	8.97E-04	1.0283	0.9359	1.12	1.0358	0.857	255/05	164/18	360/72
BC14	BC1402C	Micaschist	7.92E-04	1.018	0.9419	1.11	1.0401	0.567	269/06	177/23	012/66

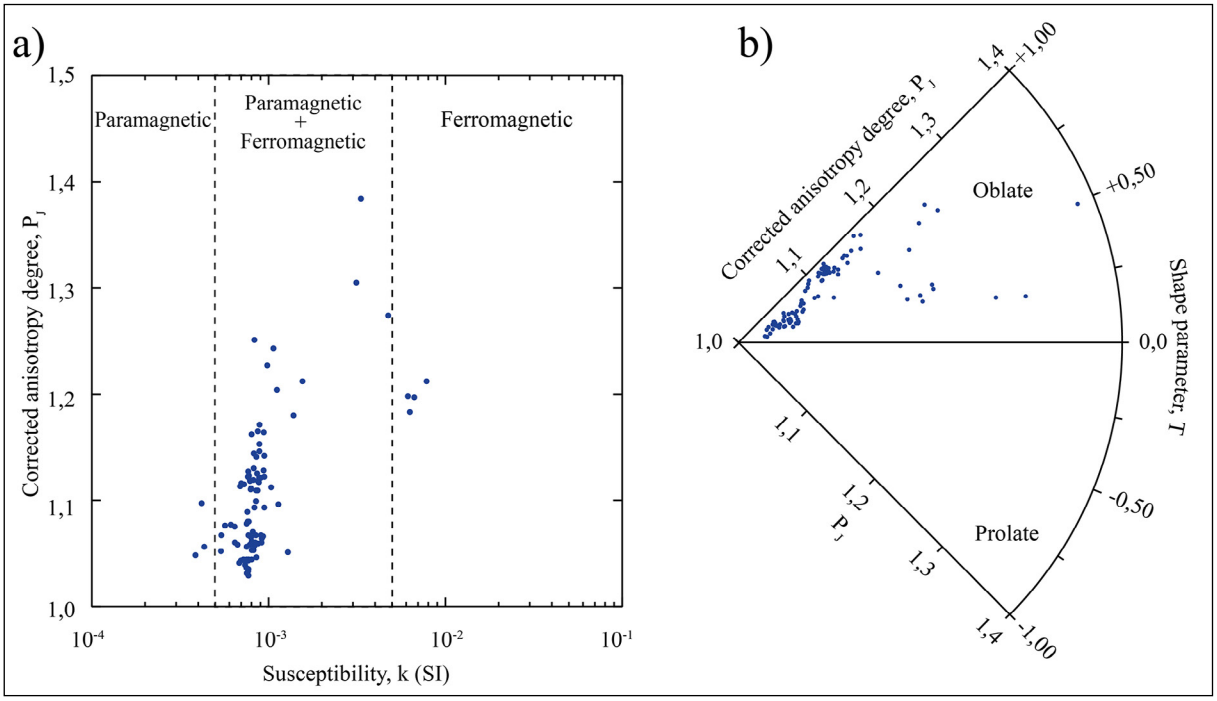

Figure 5- a) Plot of corrected anisotropy degree, P_J, against bulk susceptibility, b) Borradaile-Jackson polar plot of corrected anisotropy degree, P_J, and shape parameter, T (Jelínek, 1981; Borradaile and Jackson, 2004).

BC12. The Pearson product-moment correlation coefficient of 0.702 for this relationship exceeds the critical value of 0.2644 at the 99% confidence level (for n= 92 specimens). This relationship demonstrates that anisotropy in these rocks is controlled by the proportion of ferromagnetic versus paramagnetic contributions to the bulk susceptibility (Rochette et al., 1992), which can be implicated by variations in the relative contributions from ferromagnetic magnetite and paramagnetic amphibole in this case. Specimens from site BC12 fall outside this trend and display the largest susceptibilities encountered in this study (~7 x 10^{-3} SI), suggesting a dominant contribution from magnetite (Figure 5a) with an estimated maximum concentration of ~0.2 wt % based on bulk susceptibilities (Thompson and Oldfield, 1986).

Specimen-level data indicate the dominance of oblate fabrics, with all specimens displaying positive shape parameters (T) ranging from 0.21 to 0.96 (mean = 0.66), with no correlation between ellipsoid shape and P_J (Figure 5b). At the locality level, k_{max} axes plunge moderately to the SE (Figure 6a). They are parallel to the orientation of the macroscopic mineral lineation observed in the amphibolites in the field (Figure 6b), suggesting that the magnetic lineation represented by the k_{max} axes acts as an accurate proxy for the average orientation of elongate mineral phases in these rocks. This is confirmed by examination of oriented thin sections cut in the k_{max}/k_{min} plane that demonstrate that k_{max} axes are aligned parallel with the average orientation of the long-axes of amphibole crystals (Figure 7). k_{min} axes, representing the pole to the magnetic foliation, plunge moderately to the NW (Figure 6a) and are oriented parallel to the poles to the macroscopic metamorphic foliation (Figure 6b). The shape of the AMS at locality level may be determined using the bootstrap resampling method of Constable and Tauxe (1990). Bootstrapped eigenvectors derived from pseudo-sampling of the data are shown in Figure 8a and are tightly clustered with well-defined Kent (1982) error ellipses (Figure 8b). Cumulative distributions of the bootstrapped eigenvalues (Figure 8c) are distinct with no overlap of the bounds containing 95% of each eigenvalue, demonstrating an overall triaxial fabric within the metamorphic sole of the ophiolite (Tauxe et al., 2010).

5. Results

Thin section observations of amphibolites from the metamorphic sole of the Mersin ophiolite demonstrate an alignment of the long-axes of amphibole crystals with k_{max} axes of the AMS fabric. This relationship implies that the AMS lineation results from the development of a preferred alignment of amphibole (hornblende) crystal *c*-axes in these rocks. As such, both fabrics most likely track the finite strain in these rocks that developed at or close to their metamorphic peak. Recent experimental evidence on amphiboles

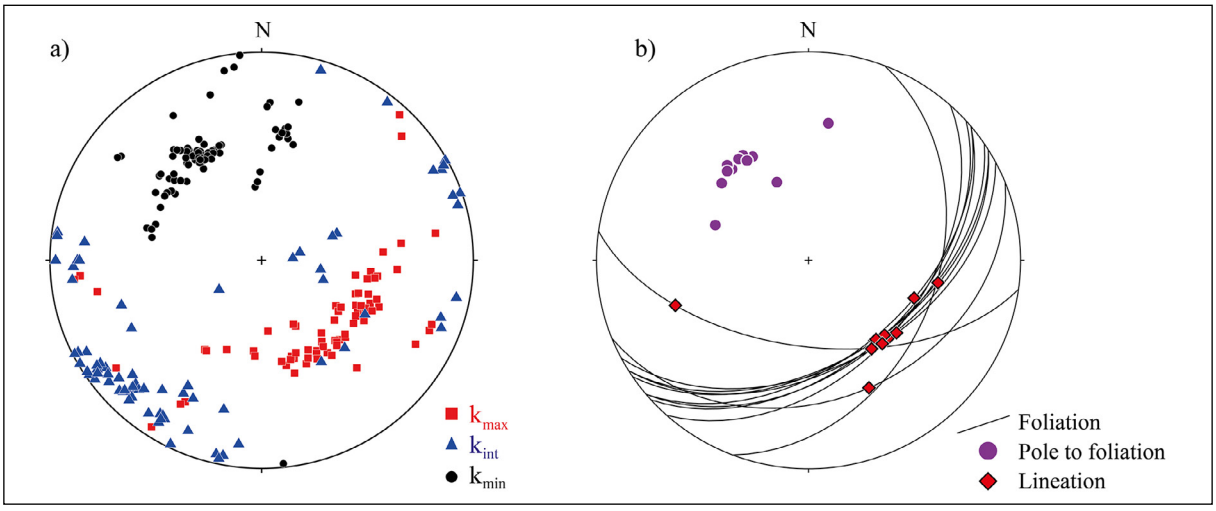

Figure 6- a) Stereographic equal area projections showing the distribution of AMS principal axes for all specimens analysed from the metamorphic sole of the Mersin ophiolite, b) stereographic equal area projections showing the orientation of the macroscopic metamorphic foliation and lineation measured in the field.

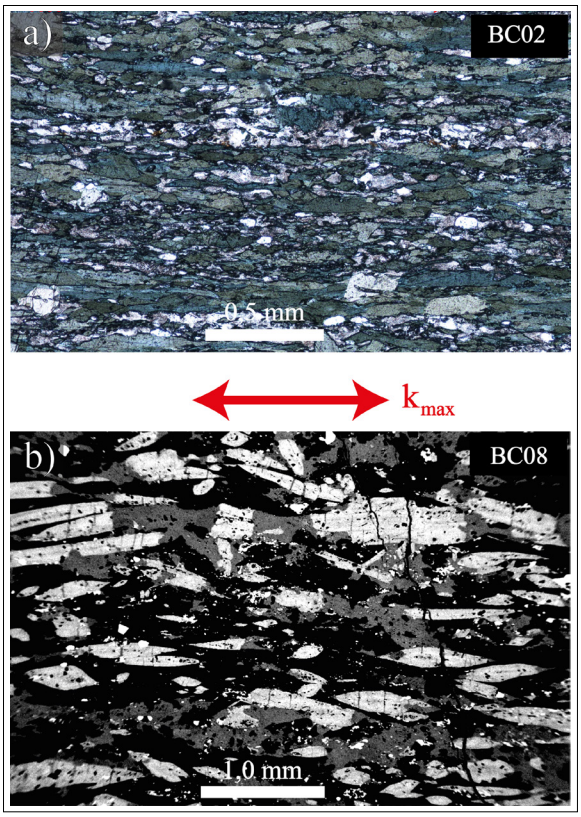

Figure 7- Photomicrograph and back-scattered electron (BSE) images of amphibolite from the metamorphic sole of the Mersin ophiolite. Thin sections are cut in the k_{max}/k_{min} plane with k_{max} parallel to the long dimension as shown; a) Thin section (plane polarised light) showing metamorphic foliation defined by the preferred alignment of blue-green amphibole, plagioclase and epidote, b) BSE image showing detail of amphibole (light shade), plagioclase (dark shade), and epidote/chlorite (intermediate shade) crystals. Note the micro-cracking (micro-boudinage) of amphibole perpendicular to the foliation (crack opening apparently parallel to k_{max}).

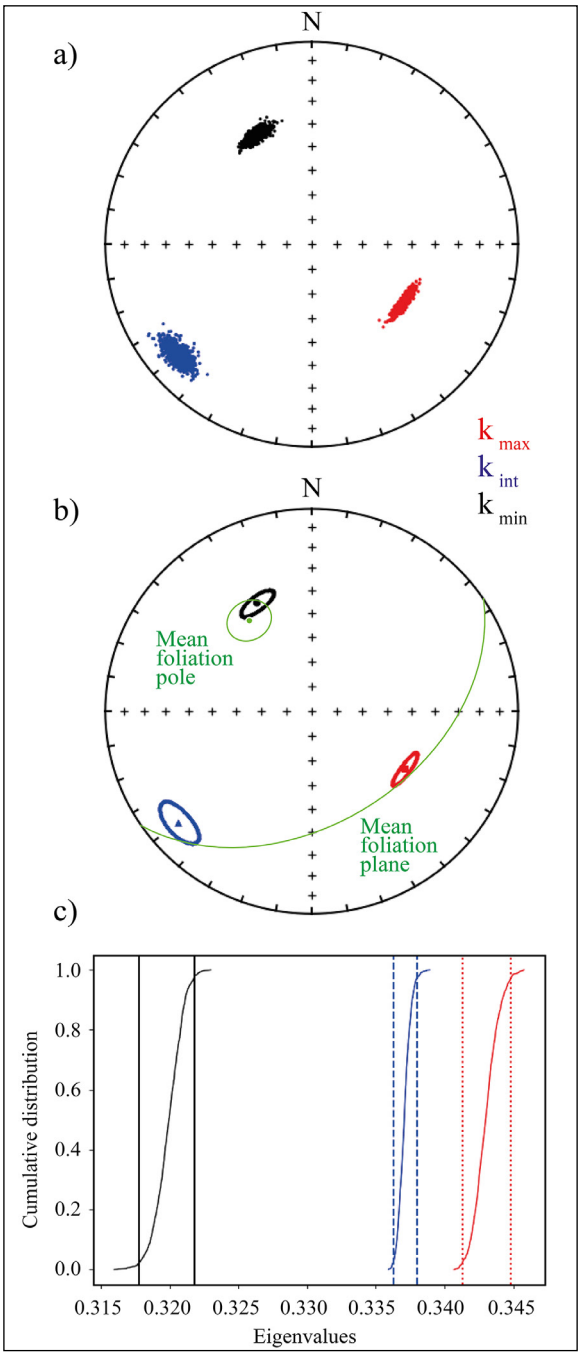

Figure 8- Bootstrap analysis of the shape of the AMS fabric in the metamorphic sole of the Mersin ophiolite, using the technique of Constable and Tauxe (1990); a) Stereographic equal-area projection of bootstrapped eigenvectors at the locality-level (geographic coordinates), b) Kent (1982) error ellipses for each distribution of eigenvectors demonstrating near-perfect alignment with the orientation of the macroscopic metamorphic fabric observed in the field, c) Cumulative distributions of the bootstrapped eigenvalues associated with the eigenvalues plotted in Figure 8a. Solid, dashed, and dotted vertical lines represent bounds containing 95% of each eigenvalue (Tauxe et al., 2010). The lack of overlap of these bounds demonstrated the presence of a triaxial fabric within these rocks.

has demonstrated that k_{max} axes in single amphibole crystals lie parallel to amphibole crystallographic b-axes, rather than their c-axes (Biedermann et al., 2015), but that preferential alignment of crystal c-axes results in bulk AMS fabrics with k_{max} axes parallel to the mineral lineation in amphibole-rich rocks (Biedermann et al., 2018). Our results suggest that there is also a contribution to the AMS fabric from minor amounts of magnetite present in the specimens. In contrast to amphibole crystals, AMS in single crystals of magnetite results from shape rather than crystallographic anisotropy (Tarling and Hrouda, 1993), with k_{max} axes normally parallel to the long-axes of magnetite crystals. An exception to

this is single domain (<1μm) magnetite crystals which have k_{max} axes parallel to their short-axis (Potter and Stephenson, 1988), leading to the development of inverse AMS fabrics. The consistency of AMS fabrics across specimens with different susceptibilities and agreement with the orientation of the metamorphic lineation seen in the field and in thin sections suggests that: i) the preferred orientation of any magnetite crystal present in the Mersin metamorphic sole rocks is coaxial with the preferred orientation of amphibole crystals; and ii) that inverse fabrics associated with single-domain magnetite are absent. Magnetite was not observed as a discrete phase during the petrographic analysis of the amphibolites, and so the inferred alignment of paramagnetic and ferromagnetic contributions to the AMS signal may reflect the presence of magnetite as an exsolution product within amphibole crystals, with their shape-preferred orientations or distribution anisotropy (Stephenson, 1994) controlled crystallographically by the amphibole lattice.

The overall triaxial AMS fabric is seen in the metamorphic sole and dominance of oblate ellipsoids at specimen-level likely reflects finite strain with a strong flattening component (producing clustering of k_{min} axes), combined with the shearing producing preferred alignment of mineral long-axes, resulting in clustering of k_{max} axes. This is consistent with the formation of the metamorphic fabric along with the upper interface of a down-going subducting plate and subsequent exhumation and accretion to the base of the Mersin ophiolite. A new tectonic model for this process, based on tectonic analysis of paleomagnetic data from the cumulate gabbros of the ophiolitic suite, mafic dykes cutting the metamorphic sole and dykes intruding the mantle sequence, was recently proposed by Morris et al. (2017) (Figure 9).

This incorporated key elements of a new mechanism for metamorphic sole formation and exhumation proposed by van Hinsbergen et al. (2015). The paleomagnetic analysis demonstrated that the

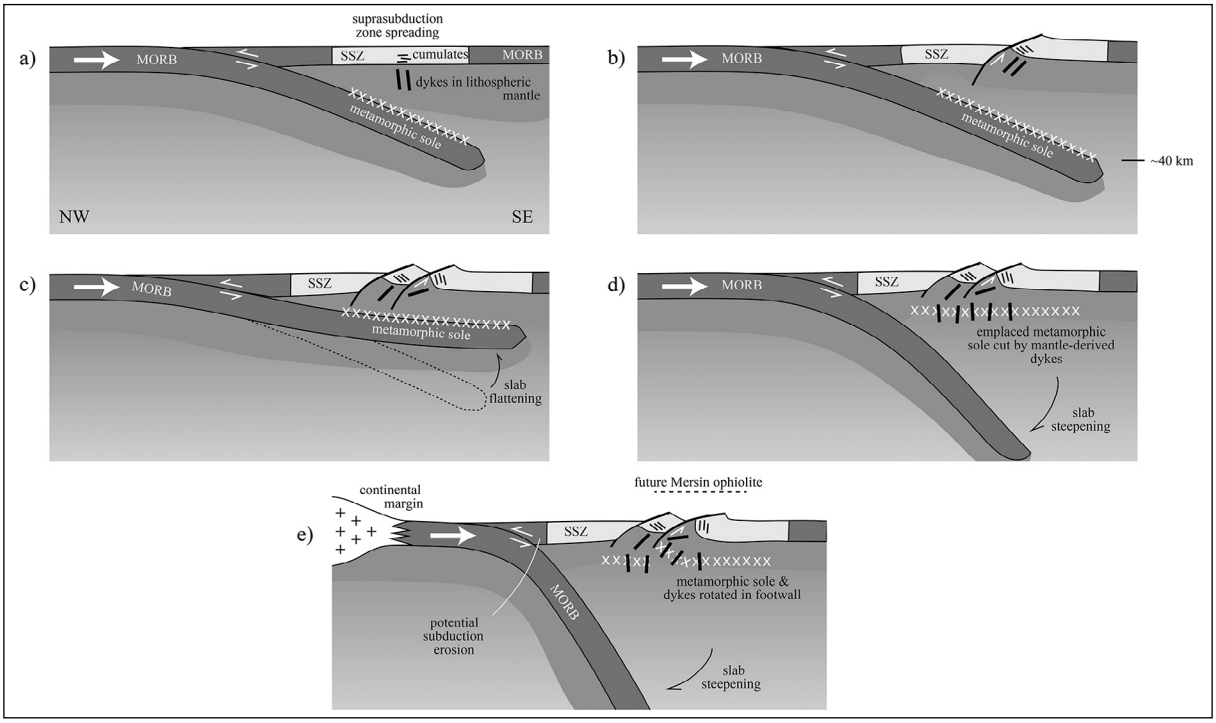

Figure 9- Conceptual model for the evolution of the Mersin ophiolite and its metamorphic sole in a fore-arc environment (modified after Morris et al., 2017); a) formation of the metamorphic sole during incipient subduction leads to the development of shear fabrics in the sole rocks, accompanied by suprasubduction zone spreading to form the Mersin ophiolite, b) tectonic rotation of the ophiolite in the footwall of an oceanic detachment fault during detachment-mode spreading, c) flattening of the down-going slab leads to the exhumation of the metamorphic sole rocks and the development of pure shear, oblate fabrics, d) accretion of the metamorphic sole to the base of the suprasubduction zone ophiolite and intrusion by mafic dykes, e) rotation of the metamorphic sole and associated dykes by capture in the footwall of an oceanic detachment fault.

Mersin ophiolite experienced major rotation around a shallowly-plunging, NE-SW-trending, ridge-parallel axis, inferred to result from rolling-hinge rotation during formation by detachment-mode seafloor spreading (Morris et al., 2017; Escartín and Canales, 2011). Dykes cutting the metamorphic sole also experienced rotation around the same ridge-parallel inclined axis but with a lower magnitude of net rotation (Morris et al., 2017). These constraints on tectonic rotation require exhumation of the metamorphic sole, accretion to the base of the overlying oceanic lithosphere before the intrusion of dykes into the sole, and subsequent capture of the sole rocks by the rotating footwall block of the oceanic detachment fault (Morris et al., 2017). This may be achieved by slab flattening in response to supra-subduction zone spreading, mantle wedge volume decrease, and upper plate extension (Figure 9; Morris et al., 2017; Van Hinsbergen et al., 2015), leading to shallowing and exhumation of the sole rocks and development of its inverted metamorphic gradient (Parlak et al., 1996). This tectonic model based on paleomagnetic tectonic rotation analysis can readily explain the magnetic anisotropy results presented here, with i) shearing along with the upper interface of the down-going slab during subduction initiation producing mineral elongation fabrics, and ii) subsequent development of strongly oblate fabrics by pure shear during flattening and exhumation of the slab and sole rocks before the accretion of the metamorphic sole to the base of the ophiolite. It is also consistent with recent interpretations of the geodynamic evolution of the metamorphic soles of other Turkish Neotethyan ophiolites (e.g. in the Beyşehir-Hoyran Nappes; Parlak et al., 2019), where exhumation is inferred to have occurred during roll-back shortly after subduction initiation.

Acknowledgements

We thank the Directorate General for Higher and Overseas Education of the Ministry of National Education, the Republic of Türkiye for the financial support provided to Buğra ÇAVDAR during his research masters (ResM) at the University of Plymouth.

References

Bascou, J., Raposo, M. I. B., Vauchez, A., Egydio-Silva, M. 2002. Titanohematite lattice-preferred orientation and magnetic anisotropy in high-temperature mylonites. Earth and Planetary Science Letters 198 (1-2), 77-92.

Biedermann, A. R., Koch, C. B., Pettke, T., Hirt, A. M. 2015. Magnetic anisotropy in natural amphibole crystals. American Mineralogist 100 (8-9), 1940-1951.

Biedermann, A. R., Kunze, K., Hirt, A. M. 2018. Interpreting magnetic fabrics in amphibole-bearing rocks. Tectonophysics 722, 566-576.

Borradaile, G. J., Hamilton, T. 2004. Magnetic fabrics may proxy as neotectonic stress trajectories, Polis rift, Cyprus. Tectonics 23 (1).

Borradaile, G. J., Jackson, M. 2004. Anisotropy of magnetic susceptibility (AMS): magnetic petrofabrics of deformed rocks. Geological Society of London, Special Publications 238 (1), 299-360.

Bouchez, J. L. 1997. Granite is never isotropic: an introduction to AMS studies of granitic rocks. Granite: From Segregation of Melt to Emplacement Fabrics, Springer, Dordrecht, 95-112.

Cañón Tapia, E. 2004. Anisotropy of magnetic susceptibility of lava flows and dykes: a historical account. Geological Society of London, Special Publications 238 (1), 205-225.

Constable, C., Tauxe, L. 1990. The bootstrap for magnetic susceptibility tensors. Journal of Geophysical Research 95, 8383- 8395.

Di Chiara, A., Morris, A., Anderson, M. W., Menegon. L., Tremblay, T. 2020. Magnetic anisotropy reveals Acadian transpressional fabrics in an Appalachian ophiolite (Thetford Mines, Canada). Geophysical Journal International 222 (2), 1034-1045.

Dilek, Y., Thy, P., Hacker, B., Grundvig, S. 1999. Structure and petrology of Tauride ophiolites and mafic dike intrusions (Turkey): implications for the Neotethyan ocean. Geological Society of America Bulletin 111 (8), 1192-1216.

Escartín, J., Canales, J. P. 2011. Detachments in oceanic lithosphere: deformation, magmatism, fluid flow, and ecosystems. Eos Transactions American Geophysical Union 92 (4).

Ferré, E., Martín-Hernández, F., Teyssier, C., Jackson, M. 2004. Paramagnetic and ferromagnetic anisotropy of magnetic susceptibility in migmatites: measurements in high and low fields and

kinematic implications. Geophysical Journal International 157 (3), 1119-1129.

Ferré, E. C., Teyssier, C., Jackson, M., Thill, J. W., Rainey, E. S. G. 2003. Magnetic susceptibility anisotropy: a new petrofabric tool in migmatites. Journal of Geophysical Research 108 (B2), 2086.

Jelínek, V. 1981. Characterization of the magnetic fabric of rocks. Tektonophysics 79 (3-4), 63-67.

Kent, J. T. 1982. The Fisher-Bingham distribution on the sphere. Journal of the Royal Statistical Society 44 (B), 71–80.

Kruckenberg, S. C., Ferré, E.C., Teyssier, C., Vanderhaeghe, O., Whitney, D. L., Seaton, N. C. A., Skord, J. A. 2010. Viscoplastic flow in migmatites deduced from fabric anisotropy: an example from the Naxos dome, Greece. Journal of Geophysical Research 115, B09401.

Martín Hernández, F., Lüneburg, C. M., Aubourg, C., Jackson, M. 2004. Magnetic fabric: methods and applications. Geological Society of London, Special Publications 238, 551.

Mattei, M., D'Agostino, N., Zananiri, I., Kondopoulou, D., Pavlides, S., Spatharas, V. 2004. Tectonic evolution of fault- bounded continental blocks: comparison of paleomagnetic and GPS data in the Corinth and Megara basins (Greece). Journal of Geophysical Research 109.

Morris, A. 2000. Magnetic fabric and palaeomagnetic analyses of the Plio-Quaternary calc-alkaline series of Aegina Island, South Aegean volcanic arc, Greece. Earth and Planetary Science Letters 176, 91-105.

Morris, A., Anderson, M. W., Omer, A., Maffione, M., Van Hinsbergen, D. J. J. 2017. Rapid fore-arc extension and detachment-mode spreading following subduction initiation. Earth and Planetary Science Letters 478, 76-88.

Morris, A., Meyer, M., Anderson, M. W., MacLeod, C. J. 2019. What do variable magnetic fabrics in gabbros of the Oman ophiolite reveal about lower crustal magmatism at fast-spreading ridges?. Geology 47, 275-278.

Omer, A. H. 2014. Integrated geophysical, geochemical, and structural analysis of the Mersin ophiolite, southern Turkey. PhD Thesis, University of Plymouth, Plymouth, United Kingdom (unpublished).

Parés, J. S. 2015. Sixty years of anisotropy of magnetic susceptibility in deformed sedimentary rocks. Frontiers in Earth Science 3, 1-13.

Parlak, O., Delaloye, M. 1996. Geochemistry and timing of post-metamorphic dyke emplacement in the Mersin Ophiolite (southern Turkey): New age constraints from $^{40}Ar/^{39}Ar$ geochronology. Terra Nova 8, 585-592.

Parlak, O., Delaloye, M. 1999. Precise 40Ar/39Ar ages from the metamorphic sole of the Mersin ophiolite (southern Turkey). Tectonophysics 301, 145-158.

Parlak, O., Robertson A. H. F. 2004. The ophiolite-related Mersin Melange, southern Turkey: its role in the tectonic– sedimentary setting of Tethys in the Eastern Mediterranean region. Geological Magazine 141, 257-286.

Parlak, O., Bozkurt, E., Delaloye, M. 1996. The obduction direction of the Mersin Ophiolite: structural evidence from subophiolitic metamorphics in the Central Tauride Belt, Southern Turkey. International Geology Review 38, 778- 786.

Parlak, O., Delaloye, M., Bingöl, E. 1995. Origin of subophiolitic metamorphic rocks beneath the Mersin ophiolite, southern Turkey. Ofioliti 20, 97-110.

Parlak, O., Dunkl, I., Karaoğlan, F., Kusky, T., Zhang, C., Wang, L., Koepke, J., Billor, Z., Hames, W. E., Şimşek, E., Şimşek, G., Şimşek, T., Öztürk, S. E. 2019. Rapid cooling history of a Neotethyan ophiolite: evidence for contemporaneous subduction initiation and metamorphic sole formation. Geological Society of America Bulletin 131, 2011-2038.

Parlak, O., Karaoğlan, F., Rızaoğlu, T., Klötzli, U., Koller, F., Billor, Z. 2013. U-Pb and ^{40}Ar-^{39}Ar geochronology of the ophiolites and granitoids from the Tauride belt: Implications for the evolution of the Inner Tauride suture. Journal of Geodynamics 65, 22-37.

Potter, D. K., Stephenson, A. 1988. Single domain particles in rocks and magnetic fabric analysis. Geophysical Research Letters 15, 1097-1100.

Rochette, P., Jackson, M., Aubourg, C. 1992. Rock magnetism and the interpretation of anisotropy of magnetic susceptibility. Reviews of Geophysics 30, 209-226.

Staudigel, H., Tauxe, L., Gee, J. S., Bogaard, P., Haspels, J., Kale, G., Leenders, A., Meijer, P., Swaak, B., Tuin, M., Van Soest, M. C., Verdurmen, E. A. Th., Zevenhuizen, A. 1999. Geochemistry and intrusive directions in sheeted dikes in the Troodos ophiolite: implications for mid-ocean ridge spreading centers. Geochemistry Geophysics Geosystems 13, 1.

Stephenson, A. 1994. Distribution anisotropy: two simple models for magnetic lineation and foliation. Physics of the Earth and Planetary Interiors 82, 49-53.

Tarling, D. H., Hrouda, F. 1993. The Magnetic Anisotropy of Rocks, Chapman and Hall, London, 217.

Tauxe, L., Butler, R. F., Banerjee, S. K., Van der Voo, R. 2010. Essentials of Paleomagnetism, University of California Press, Berkeley, California, 500.

Tekin, U. K., Bedi, Y., Okuyucu, C., Göncüoglu, M. C., Sayit, K. 2016. Radiolarian biochronology of upper Anisian to upper Ladinian (Middle Triassic) blocks and tectonic slices of volcano-sedimentary successions in the Mersin Mélange, southern Turkey: new insights for the evolution of Neotethys. Journal of African Earth Sciences 124, 409–426.

Thompson, R., Oldfield, F. 1986. Environmental Magnetism. Allen and Unwin, London, 227.

Van Hinsbergen, D. J., Peters, K., Maffione, M., Spakman, W., Guilmette, C., Thieulot, C., Kaymakcı, N. 2015. Dynamics of intraoceanic subduction initiation: suprasubduction zone ophiolite formation and metamorphic sole exhumation in context of absolute plate motions. Geochemistry, Geophysics, Geosystems 16 (6), 1771-1785.